2022 IEEE Texas Symposium on Wireless and Microwave Circuits and Systems (WMCS) | 978-1-6654-8609-5/22/$31.00 ©2022 IEEE | DOI: 10.1109/WMCS55582.2022.9866434

Spintronics Technology Solutions for Interferometric Thermal-Electromagnetic Sensing

S. Wane[$], Q.H. Tran [$], T.V. Dinh[$], J. A. Eddine[$], F. Duffourg[$], F. Ndagijimana[#], D. Bajon[$], F. Terki[$], J. Rioult [#, Λ], J.-L. Darroman[Λ], L. Bonnaire[Λ], O. Montfort[*], V. Huard[*], J.-P. Raskin[†], D. Lederer[†], A. Bousseksou[§]

[$]eV-Technologies,[Λ]Luxondes, [#] G2ELab Grenoble, [Λ] UGE Lille, [*]Dolphin-Design, [†] ICTEAM-UCL, [§]LCC-CNRS

***Abstract*— Hybrid electromagnetic (EM) and thermal imaging using spintronic technologies is proposed for sensing circuits and systems in near-field and far-field from DC (*Switching-Power*) to mmWave frequencies. High resolution spintronic sensors capable of detecting magnetic fields ranging from few tens of mT (*milli-Tesla*) down to tens of pT (*pico-Tesla*) are demonstrated spanning about 10 orders of magnitude in dynamic range. A configurable *Agile Front-End-Module LNA* (AFEM) is combined with spintronics probe-array sensors providing adjustable 80 dB of dynamic range for subsequent processing of MIMO correlations in time and frequency domains. The proposed *hybrid EM-Thermal sensing* solution is applied to mmWave beamforming modules demonstrating the possibility of extracting *power-density* and *energy-density* metrics as a function of beamforming angles. An infrared (IR)-Visual dual-camera is introduced together with augmented reality (AR) based on 3D *non-uniform spatial-sampling*. Porting of chemically functionalized spintronic sensing materials into advanced FD-SOI platforms is proposed using advanced MRAM/SRAM process technologies.**

Keywords— Spintronic, Correlation Technologies, Hybrid EM-Thermal Sensing, IR-Visual camera, MRAM/SRAM, FDSOI, Augmented Reality (AR), configurable FEM.

I. Introduction

Spintronics [1-9] is associated with the invention of the giant magnetoresistance (GMR) effect in 1988 by Fert [1] and Grunberg [2] who received the 2007 Nobel Prize in Physics. Spintronic-based devices use the electron's spin degree of freedom, which leads to very promising performance. The industrial deployment of the technology started in the 1990s with the development of highly sensitive GMR read sensors for hard disk drive (HDD) applications. In 1995, two groups − one in the USA (MIT) and the other in Japan (Tohoku University) − separately demonstrated about 20% tunnel magnetoresistance (TMR) with an AlOx barrier at room temperature which led to solid-state random access memory technology solutions. These important discoveries drove the evolution in the process and architecture of perpendicular magnetic tunnel junctions (pMTJs) for spin transfer torque magnetic random access memory (STT-MRAM) devices [8-9]. The resulting technology evolutions open new avenues toward reconfigurability and non-volatile memory for in-memory computing architectures, adaptive logic computing and neuromorphic computing (AI). All these technological achievements were made possible by overcoming critical challenges in conjunction with materials, processes and active circuits co-design and co-integration. In a recent publication [7], we have presented a new high resolution very-near-field (VNF) probe-array for hybrid magnetic and thermal sensing with micronic spatial resolution using high-sensitivity spintronic sensors for near-field magnetic-sensing of electronic circuits and radiating systems.

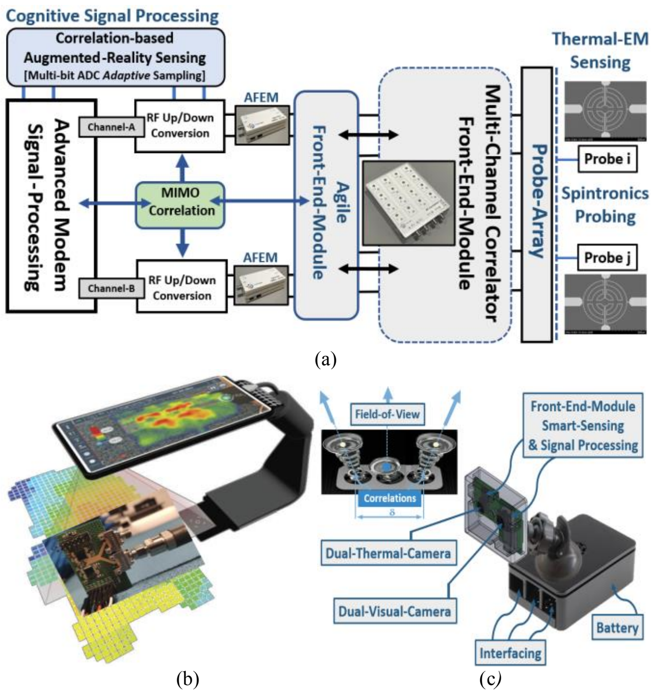

Fig.1: Configurable AFEM (*Agile Front-End-Module*) combined with spintronic sensors providing adjustable 80 dB dynamic range for MIMO correlations (a) of stochastic signals. Augmented reality (AR) based on 3D non-uniform spatial-sampling (b). Infra-Red (IR)-Visual dual-camera (c).

In this contribution, we present a new development on the practical use of industrialized spintronics-based sensors for very near-field measurements of electronic circuits and radiating systems with focus on the following attributes:

- *Configurable FEM* (LNAs, PAs, switches, ADCs, etc...) providing adjustable 80 dB dynamic range with a multi-channel RF correlator module combined with spintronics probe-array sensors (Fig.1(a)).
- *Hybrid Thermal-EM* unified correlations using an IR-Visual dual-camera (Fig.1(c)) with augmented reality (Fig.1(b)) based on 3D non-uniform spatial sampling.

II. Main Results, Analysis and Discussion

A. *Spintronics Configurable RF Correlator with AFEM*

The proposed spintronic magnetic sensors can be hybridized with spin crossover [6] functionalized materials toward Thermal-Electromagnetic interferometric sensing [7]. Fig. 2 depicts the roadmap for spintronic sensors sensitivity toward functionalized cognitive materials. The roadmap shows sensitivities in the *pico-Tesla* range with the prospect of performances reaching the *femto-Tesla* range, which is currently only accessible through SQUID (*superconducting quantum interference device*) technologies (Fig. 2(a)).

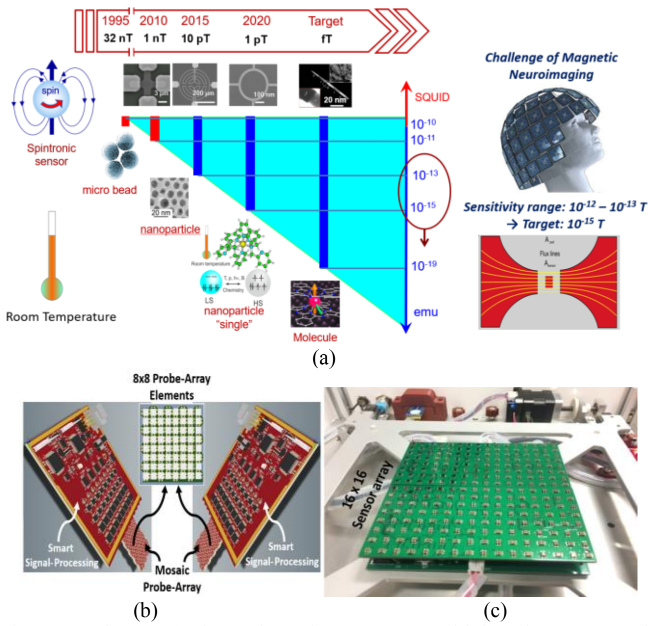

Fig.2: Roadmap (a) for Spintronic sensors sensitivity [in T] toward functionalized cognitive materials. 8x8 spintronic sensor-array (b), 16x16 sensor-array (c) for measuring radiated EM fields.

Fig. 2(b) and Fig. 2(c) show 8x8 and 16x16 spintronic sensor-arrays for very near-field sensing of radiated EM fields. Sensitivity at the Femto-Tesla range is required in order to deal with brain induced magnetic field levels while sensitivity in the Pico-Tesla range will be sufficient to detect magnetic fields radiated by the human heart [10]. The challenge of reaching such low magnetic fields is not only a question of sensitivity but also a requirement of low-noise levels. Unified co-integration of analog FEMs (active circuitry such as LNAs, PAs, switches, ADCs, etc...) with spintronics, including advanced DSP, is proposed through the porting of spintronics hybrid Thermal-EM sensing into advanced Fully Depleted Silicon-On-Insulator (FD-SOI) platforms [11] using an ASIC-based System on a Chip (ASIC-SoC) technology solution. The agile front-end-module low noise amplifier (LNA) is a dynamic stage that can be configured to operate over 7 distinct bands spread over the range 10MHz to 30GHz: C_1: 10MHz – 30GHz, C_2: 15 – 30GHz, C_3: 6 – 12GHz, C_4: 5.5 – 8.5 GHz, C_5: 3.5 – 7GHz, C_6: 2 – 5 GHz, C_7: 10MHz – 3GHz. The LNA also features a wide full band mode. Each band offers excellent out of band filtering. The higher bands from 8GHz to 30 GHz offer tunable filters that can be reconfigured to remove any unwanted products. The lower bands are split equally into band pass filters. For each band the gain can be adjusted from +40dB to -40dB. The LNA has an integrated power detector that can be used to detect compression. The LNA is also thermally compensated by an oven and temperature sensor to ensure excellent gain stability over time.

In Fig. 3(a), comparisons between measured and simulated magnetic fields (a) in near-field [12-14], at 2.45GHz, 5GHz, 6GHz, 8.75GHz, 9.7GHz are presented showing excellent agreement for a 10dBm power level. In Fig. 3(b) three different measurement campaigns are conducted to assess the repeatability of the measurement accuracy in open-space conditions (*without absorbers*) with adjustable DUT-to-Probe (Fig. 3(c) and Fig. 3(d)) distance. Extracted power-density as a function of source power-levels at 0dBm, 5dBm, 10dBm, 15dBm and 20dBm is shown in Fig. 3(e).

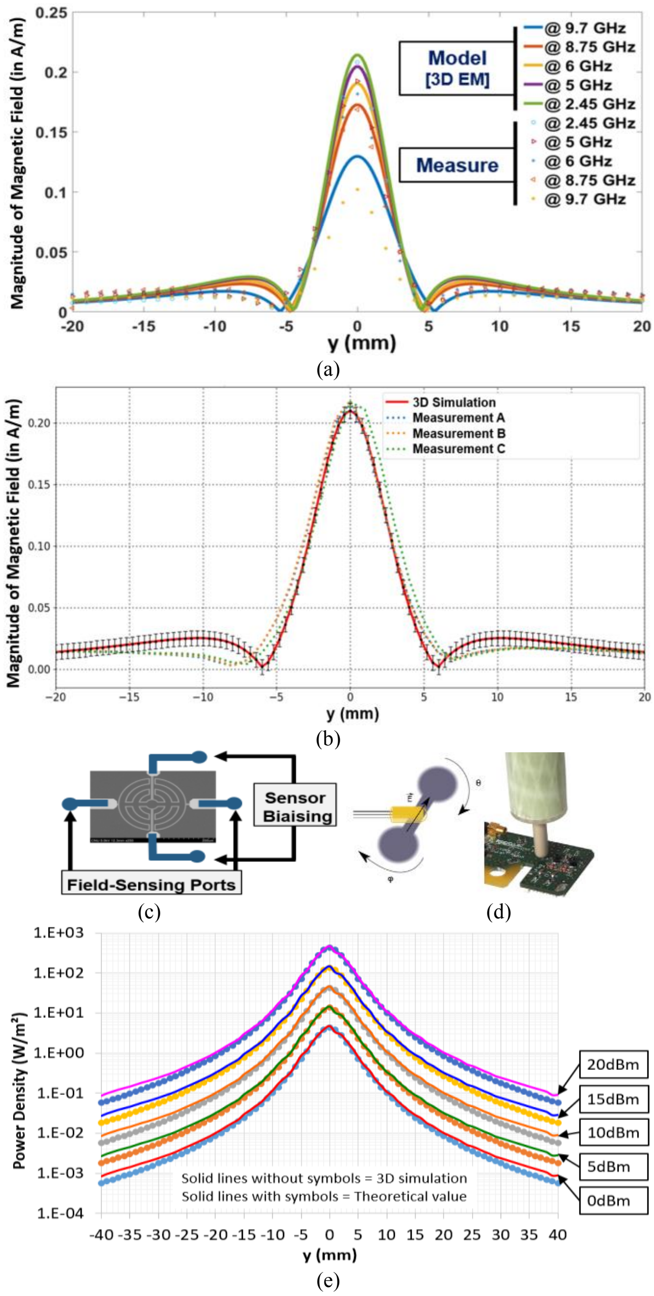

Fig.3: Measured versus simulated (a) magnetic field in near-field (*2mm from the PCB module*) at 2.45GHz, 5GHz, 6GHz, 8.75GHz, 9.7GHz and assessment of measurement repeatability in open-space conditions (b). Spintronic sensor using 4-terminal (c) with adjustable DUT-to-Probe distance and electro-optical (*Kapteos technologies*) probe (d). Extracted power-density (e) as function of source power-levels at 100MHz.

For the time domain measurements, the output voltages $v_A(t)$ and $v_B(t)$, in Fig.4(a)(b), are the result of the convolution (*operation * in equation (1)*) of the pulse generator signal $v_{in}(t)$ with the impulse responses $H_{Channel-A}(t)$ and $H_{Channel-B}(t)$ of the two channels A and B which encompasses the response of the spintronic probes and the channels between the output of the generator and the oscilloscope inputs (*channels A and B*) in Fig.4(b). Thus, the output voltages $v_A(t)$ and $v_B(t)$ are directly influenced by the noise contributions $n_A(t)$ and $n_B(t)$ which account for thermal noise and electromagnetic couplings. Hence, we obtain:

$$\begin{aligned} v_A(t) &= v_{in}(t) * H_{Channel-A}(t) + n_A(t) \\ v_B(t) &= v_{in}(t) * H_{Channel-B}(t) + n_B(t) \end{aligned} \quad (1)$$

The noise terms are assumed uncorrelated with each other and with the received signals at channels A and B. The signal source generates a waveform (gaussian pulses or train of rectangular shaped pulses, each with period T). The impulse responses both from the generator and a single spintronic probe, based on averaged values of the measured signals, are shown in Fig. 5. The design of the spintronic probes minimizes their invasiveness to the EM field. Dedicated calibration modules are developed for relating the probes sensed signals to the actual EM field components in time and frequency domains. For noise correlations analysis, time-domain calibration are conducted for broadband characterizations of stochastic EM fields.

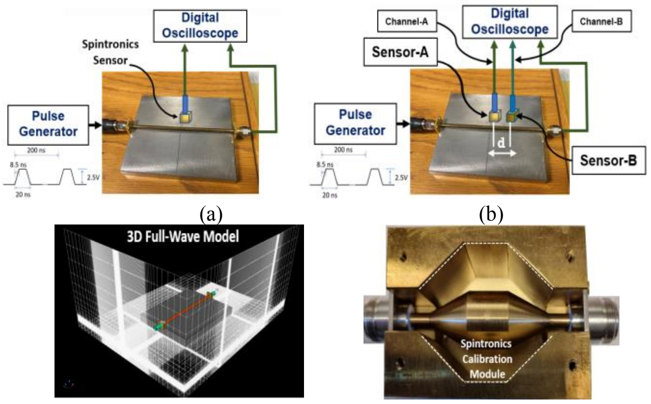

Fig.4 TL-DUT with single (a) and dual-probes for near-field experimental setup (b). 3D Full-Wave model (c). Spintronic calibration module (d).

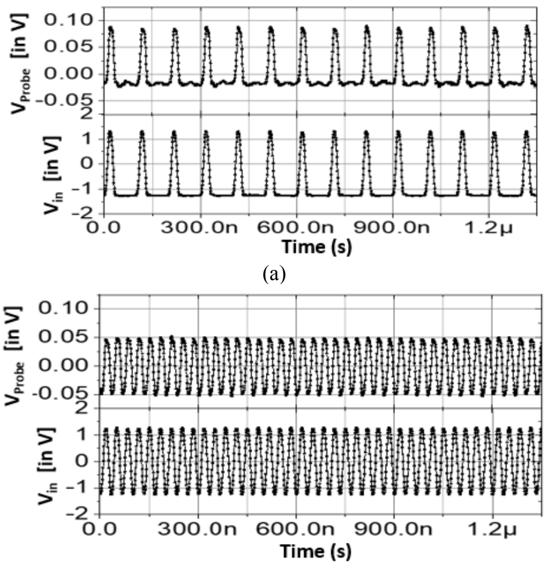

Fig.5 Measured time-domain response of reference signal generator and Spintronics single sensor in near field using two-port oscilloscope at 10MHz (a) and 30MHz (b).

Two-Point field-field correlations is known to provide a full description of noisy electromagnetic fields. The *Two-Point* experimental setup shown in Fig.4(b) is used to extract Green's functions in time-domain which can be linked to auto-correlation and cross-correlation functions. Stationary stochastic electromagnetic fields with Gaussian probability distribution can be fully extracted using their Green's functions based auto-correlation and cross correlation of all electric and magnetic field components in time-domain. Fig.5 shows the measured time domain responses of the Two-Point sampling spintronic probes. The electric-field and the thermal heatmap distributions at 2 mm from the DUT are shown in Fig.6(b) and Fig.6(c) respectively. The used spintronic sensors can be hybridized with spin crossover functionalized materials [6-7] toward Thermal-Electromagnetic interferometric sensing.

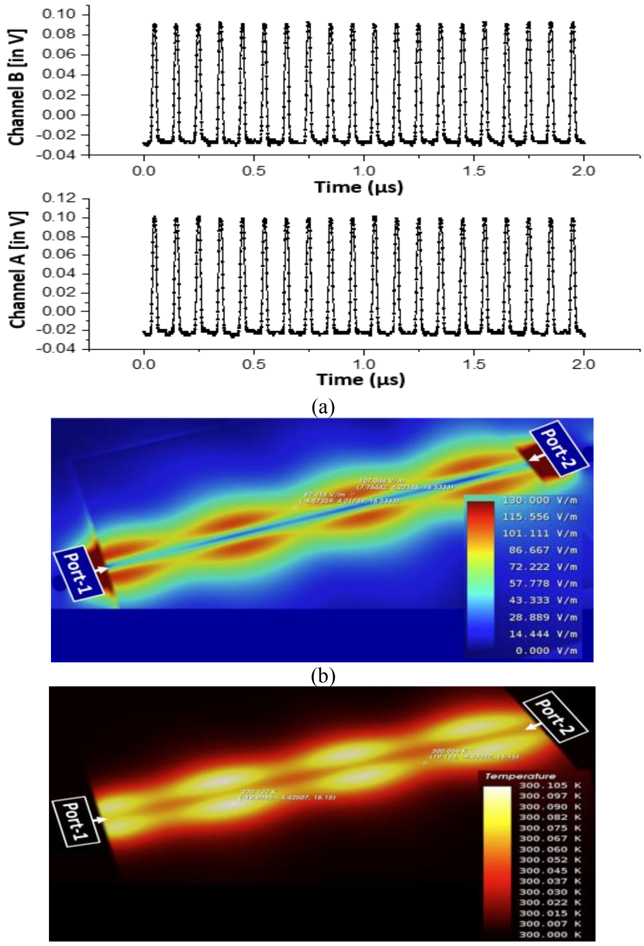

Fig.6 Measured Dual-Channel (A & B) time-domain response of Spintronics sensor in near field using two-port oscilloscope. Electric field (b) and Thermal heatmap (c) distributions at 5.8GHz at 2 mm from the DUT.

B. *Spintronics-based Interferometric EM-Thermal Near-Field Sensing Using Power and Energy Density Metrics*

The use of electromagnetic infrared techniques for visualizing and measuring microwave fields is well known [15-18], following the pioneering work of Hasegawa [19] in 1995. The available techniques consist in inserting sensitive films with electric and/or magnetic properties, which induce currents resulting in heating recorded by the infrared cameras. However, today, to our best knowledge, available solutions are based on materials that demand high input powers up to several tens of dBm which lead to low heating effects that are very difficult to use for OTA-Testing of devices and systems. We propose alternative solutions based on the use of quantum spin-crossover (SCO) materials [6-7] exhibiting functional properties which are responsive to multi-physics external stimuli such as temperature, pressure, light irradiation, electromagnetic field, radiation, nuclear decay, soft-X-ray, (de)solvation.

We introduce new Electromagnetic-Thermal sensing solutions using SCO materials for near-field and far-field characterization of electronic circuits and radiating systems. Use of innovative correlation technologies [20] is combined with advanced interferometric synchronized sampling for accurate extraction of vectorial power and energy density metrics in time and frequency domains. In Fig. 7(a)-(b), two separate functionalizations are considered distinctly for the coating of the SCO material on the DUT side and on the IR/Visible camera side.

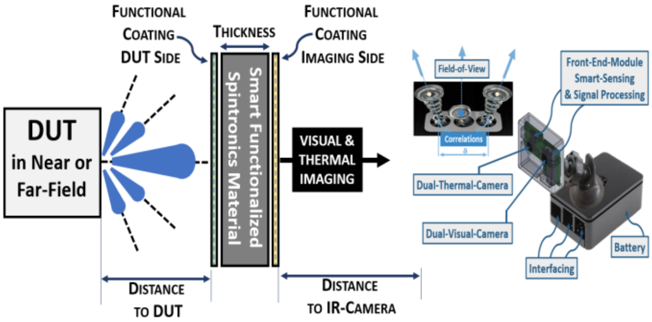

(a)

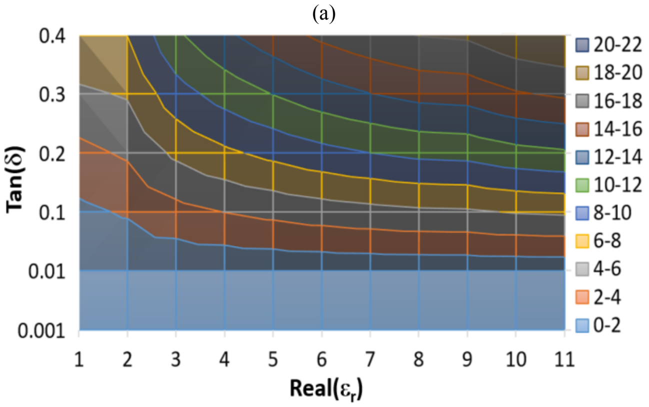

(b)

Fig. 7: Smart functionalized spintronics material for EM-Thermal sensing using IR-Camera (a). Thermal variations as function of SCO material complex permittivity (b).

Fig. 7(b) presents thermal variations as a function of the complex permittivity of the SCO material. The proposed EM-Thermal sensing solutions are evaluated using a 5G-NR FR2 8x8 elements phased array module (Fig. 8(a)) as DUT for frequencies in the band from 26 GHz to 30 GHz.

It is observed that a direct link can be established between the thermal variations on the indicator material and the square of the electric (or magnetic) field. Few tens of dBm input power feeding the radiating elements will lead to few degrees heating dynamic on the used thermal indicator from which field amplitudes can be deduced following simple relations:

- *For Electric-Field as primary sensing field:*

$$|E| = \mathrm{X}^{\mathrm{E}}_{\mathrm{EM-Thermal}}\sqrt{\Delta T_{Averaged}} \quad (2)$$

- *For Magnetic-Field as primary sensing field:*

$$|H| = \mathrm{X}^{\mathrm{H}}_{\mathrm{EM-Thermal}}\sqrt{\Delta T_{Averaged}} \quad (3)$$

In equations (2) and (3) $\mathrm{X}^{\mathrm{E}}_{\mathrm{EM-Thermal}}$ and $\mathrm{X}^{\mathrm{H}}_{\mathrm{EM-Thermal}}$ are conversion coefficients that depend on the heat transfer coefficient, the heat capacity, the density of the thermal indicator material, and the frequency. From equations (2) and (3) the power density (*spatially averaged*) appears in the form:

$$|sPD| = \propto \mathrm{X}^{E}_{EM-Thermal}\mathrm{X}^{H}_{EM-Thermal}\Delta T_{Averaged} \quad (4)$$

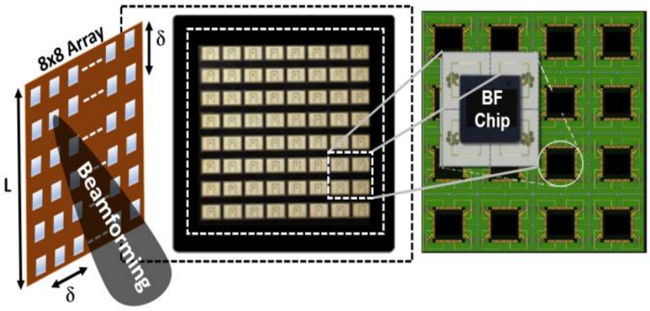

(a)

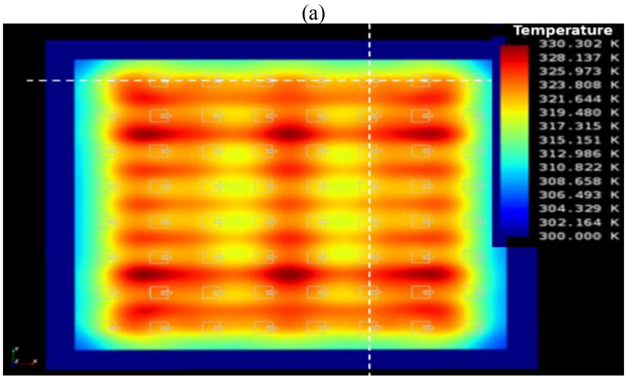

(b)

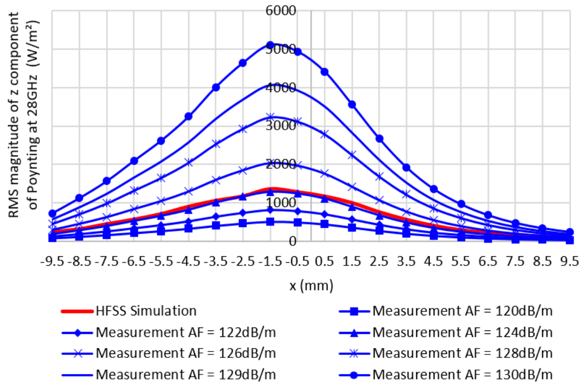

(c)

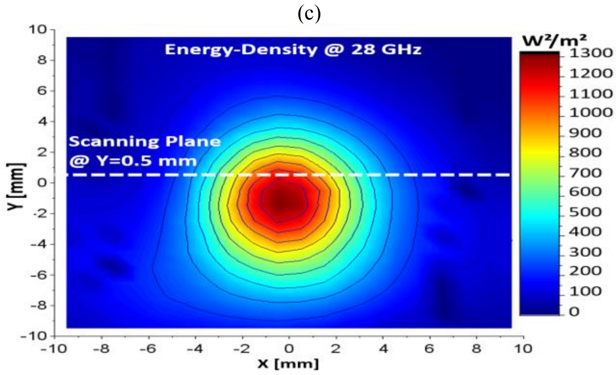

(d)

Fig.8: Phased-array DUT for FR2 band (a) and extracted thermal heatmaps (b) using SCO sensing material. Power-density (c) of unitary antenna element: measurement versus 3D simulations at 28 GHz for reference scanning plane at Y=0.5 mm (c). Energy-density, 6mm from the DUT, at 28 GHz (d).

The power transfer process from electromagnetic fields to thermal power dissipation is better described by a transient phenomenology which directly depends on the material's properties (*e.g., mass m, thickness, specific thermal capacity*). The underlying physical analysis can be carried out using the Stefan–Boltzmann law for black body radiators formulated in time-domain. Challenges of such time-domain analysis reside in proper representation of complex

permittivity of SCO materials fulfilling passivity and causality preservations beyond the classical Maxwell-Garnett model.
Fig.8(b) shows the thermal heatmaps extracted at 2mm distance from the phased-array module. Measured energy-densities in near-field with different antenna-factor (AF) values (*from 120dB/m to 130dB/m*) with variable sensitivity from the DUT at 28 GHz with 23 dBm input power are compared to 3D EM simulations (HFSS) in Fig. 8(c). Fig. 8(d) presents the extracted energy-density, 6 mm from the DUT, at 28 GHz.

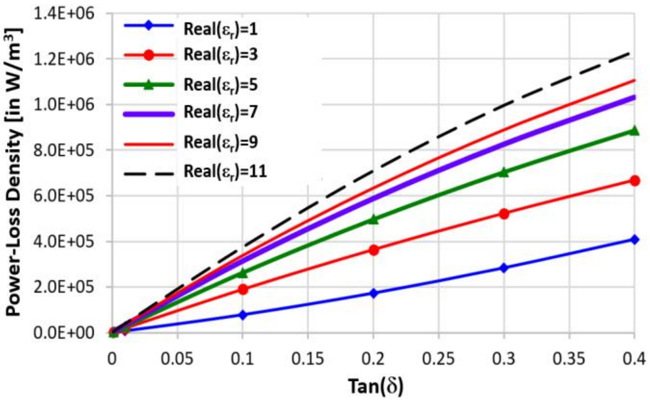

Fig.9: Simulated power-loss density (*in W/m³*) in the indicator material as a function of dielectric losses (*Tan(δ)*) of the SCO material at 28 GHz for different values of the relative permittivity.

The observed direct link between the variations of the heatmaps on the indicator material and the values of the complex permittivity highlights the ability to engineer the SCO material for optimal EM-Thermal conversion accuracy. Fig.9(a) depicts the simulated power-loss density (in /m^3) occurring in the indicator material as a function of the dielectric losses (*Tan(δ)*) of the SCO material at 28 GHz for different values of the relative permittivity. Macro-modeling effective electrical properties of composites is essential for simultaneously co-designing electromagnetic properties with mechanical and thermal material properties through a multi-physics approach. Although electromagnetic performances of materials are very important for the functional specifications of the end-product, constraints resulting from manufacturing process and thermal-mechanical considerations can be discriminating from application perspective. Among main thermal-electrical parameters of interest are effective permittivity, effective permeability, effective conductivity, and effective heat conductivity. Ferro-electric materials are such that their permittivity can be modified by a biasing electric field with a nonlinear dependence. Ferro-polymer materials offer flexibility for tunability and reconfigurability. State-of-the-art macro-modeling methods for extracting effective electrical properties of composite materials include analytical or semi-analytical techniques derived using closed-form expressions (*mixed equations*) and numerical solutions based on full-wave Maxwell equations. Available analytical or semi-analytical methods [22-23] for determining the effective complex permittivity of composite materials include the following approaches based on mixing-equations: Maxwell-Garnett's, Lichtenecker's, Bruggeman's, Buchelnikov's , Ignatenko's models.

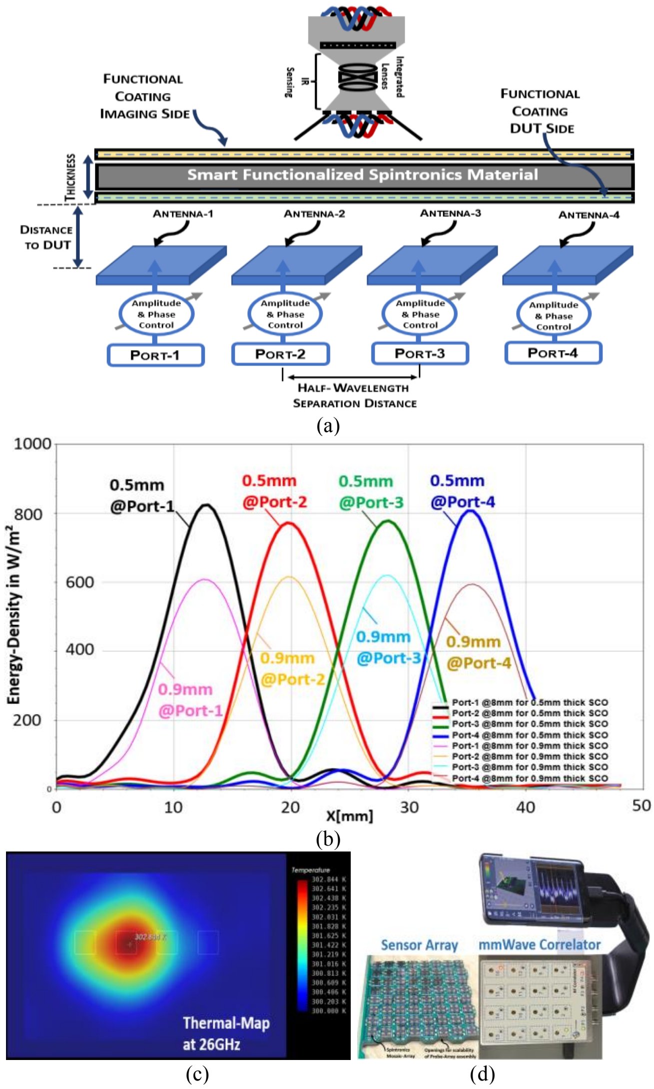

Fig.10: Experimental 1x4 antenna array (a). Energy-Density at 26 GHz extracted from Thermal heatmaps for 0.5 mm and 0.9 mm thick SCO indicator materials (b). Thermal heat map when Port-2 is excited (c). EM-Scanphone 3D visualization (d) interface connected to 8x8 spintronic sensor array.

Fig.10(b) and Fig.10(c) respectively present extracted energy-density and thermal distribution at 26 GHz for a 1x4 antenna elements module (Fig.10(a)). The used optimal EM-Thermal conversion leads to high-sensitivity functionalization [21] of the spintronics indicator material for imaging EM fields through their thermal signatures using both IR and Visible imagers. The correlation of Thermal and EM imaging streams uses advanced 3D augmented reality [22] based on non-structured spatial sampling (*non-uniform FFT custom algorithms*). The *non-structured spatial sampling* can be combined with 3D near-field and far field scanning of stochastic EM field for building new OTA testing (Fig.11(a),(b),(c)) solutions [25] with the following functionalities:

- *Ambiant-Noise Cancellation (ANC) solutions using correlation technologies.*
- *Correlation-aware Multi-Physics Thermal-EM scanning solutions.*
- *Wave-Shaping Solutions accounting for stochastic-noise propagation.*
- *Time-reversal Algorithms for stochastic fields back-propagation.*

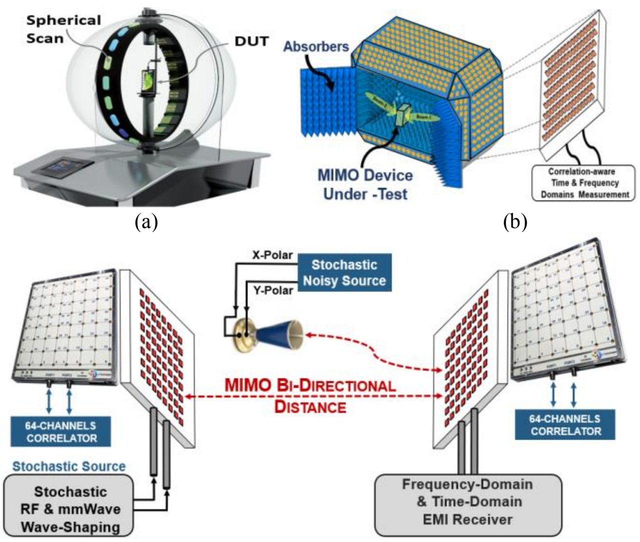

(c)

Fig.11: 3D spherical scanning system to be combined with eV-Technologies RF/mmWave correlator modules (a). OTA chambers integrating eV-Technologies correlator modules (b). MIMO Tx-Rx system (c) using RF/mmWave correlator modules combined with broadband EMI receivers.

III. CONCLUSION

Hybrid EM and thermal imaging using Spintronic technologies has been presented for sensing near-field and far-field radiations emitted by RF and mmWave circuits and systems. A configurable AFEM (*Agile Front-End-Module*) is combined with spintronics probe-array sensors providing adjustable 80 dB of dynamic range for broadband sensing of MIMO systems accounting for channel-to-channel correlations in time and frequency domains. The proposed hybrid EM-Thermal sensing solutions are applied to Sub-10 GHz carrier applications and to mmWave beamforming modules demonstrating the possibility of extracting power-density and energy-density as a function of near-field distances separating the DUT from the probing system. Infra-Red (IR)-Visual dual-camera is introduced together with augmented reality (AR) based on 3D *non-uniform spatial-sampling* for systematic extraction of near-field EM-Thermal heatmaps. Porting of spintronics hybrid Thermal-EM sensing into advanced FD-SOI platforms is proposed. The capabilities of the FDSOI processes for the integration of MRAM/SRAM will enable new spintronics sensing solutions beyond classical information storage applications. Using spin-transfer torque (STT) for modulating RF generation and detection in time and frequency domains, combined with the implementation of random generator arrays, will facilitate the unification of IoT and RF technologies *(unified solution covering frequencies from DC to mmWave*). The co-integration of SCO materials with configurable FEMs will foster new possibilities for replacing conventional IR-imagers by low-cost sensors with fluorescent functionalization processes. The resulting functionalization processes will support new hybrid EM-Thermal architecture solutions capable of *time-reversal* depth analysis for emerging applications. Nanomaterials engineering will yield further developments beyond [26] the performances of classical [27] heat transfer mechanisms. Use of *higher-order (cumulants)* correlation technologies [20] will create unifying bridges between partially [28] coherent stochastic EM fields and Thermal heat exchanges between bodies at multiscale levels (*down to nanometric resolutions*).

REFERENCES

[1] A. Fert, Nobel Lecture: Origin, development, and future of spintronics. Rev. Mod. Phys. 80, 1517–1530 (2008).

[2] A. Fert, P. Grunberg, et al., "Layered magnetic structures: interlayer exchange coupling and giant magnetoresistance," Journal of Magnetism and Magnetic Materials, vol. 140-144, pp. 1–8, 1995.

[3] Locatelli N., Cros V. & Grollier J. "Spin-torque building blocks". Nat. Mater. 13, 11–20 (2014). [PubMed: 24343514].

[4] Garcia-Sanchez, F., Sampaio, J., Reyren, N., Cros, V., Kim, J.-V.: A skyrmion-based spin-torque nano-oscillator. New J. Phys. 18(7), 075011 (2016).

[5] P.P. Freitas, P.P et al., "Spintronic Sensors", Proc. IEEE 2016, 104, 1894–1918, doi:10.1109/ JPROC.2016.2578303G.

[6] Molnár, M. Mikolasek, K. Ridier, A. Fahs, W. Nicolazzi, A. Bousseksou, "Molecular Spin Crossover Materials: Review of the Lattice Dynamical Properties", Annalen Physik 2019, 531, 1900076.

[7] S. Wane, Q. Tran, et al., "High Resolution Spintronics Probe-Array Technology Solutions for Very Near-Field Scanning", in Proceedings of the 2021 IEEE Conference on Antenna Measurements & Applications, Antibes Juan-les-Pins, France, 15–17 Nov. 2021.

[8] J. S. Moodera, L. R. Kinder, T. M. Wong, and R. Meservey, Phys. Rev. Lett. 74, 3273 (1995).

[9] T. Miyazaki and N. Tezuka, J. Magn. Magn. Mater. 139, L231 (1995).

[10] G. M. Baule and R. McFee, "Detection of the magnetic field of the heart," Am. Heart J. 66, 95–96 (1963).

[11] Bich-Yen Nguyen, et al., "A Path to Energy Efficiency and Reliability for ICs: Fully Depleted Silicon-on-Insulator (FD-SOI) Devices Offer Many Advantages", IEEE Solid-State Circuits Mag. (Volume: 10, Issue: 4 , Fall 2018).

[12] Bolomey, J.C., et al., "Rapid Near-Field Antenna Testing via Arrays of Modulated Scattering Probes," IEEE Trans. on Ant. and Prop., vol. 36, no. 6, pp. 804-814, June 1988.

[13] Bolomey, J.C. and F.E. Gardiol, Engineering Applications of the Modulated Scatterer Technique, Artech House, Norwood, MA, 2001.

[14] B.Fourestie, J.-C. Bolomey, et al., "Spherical Near Field Facility for Characterizing Random Emissions", IEEE Trans. On Ant. and Prop., Vol. 53, no. 8, pp. 2582-2588, August 2005.

[15] P. Levesque and L. Leylekian, "Capteur vectoriel de champs électromagnétique par thermographie infrarouge," French Patent 9 816 079, Dec. 17, 1998.

[16] D. Prost, et al., "Infrared Thermography of Microwave Electromagnetic Fields", D, EMC Europe, Rome, (2012).

[17] H. Ragazzo, et al., "Detection and imaging of magnetic field in the microwave regime with a combination of magnetic losses material and thermofluorescent molecules," IEEE Trans. Magn., vol. 55, no. 2, pp. 1–4, Feb. 2019.

[18] C. Baer, K. Orend, B. Hattenhorst, T. Much, "Field Representation Microwave Thermography Utilizing Lossy Microwave Design Materials". Sensors 21(14): 4830 (2021).

[19] T. Hasegawa, "A new method of observing electromagnetic fields at high frequencies by use of test paper", Bull. Yamagata Univ. IV, Japan, 1995.

[20] S. Wane, et al., "Correlation Technologies for OTA Testing of Mobile Devices: Power-Density Measurement", in IEEE Conf. on Ant. Measurements Applications, Nov. 2021.

[21] S. Wane, Q.H. Tran, et al., "Smart Sensing of Vital-Signs: Co-Design of Tunable Quantum-Spin Crossover Materials with Secure Photonics and RF Front-End-Module", IEEE-MTT-Texas symposium 2021.

[22] J.C. Maxwell Garnett, "Colours in metal glasses and metallic films," Phil. Trans. Royal Soc. London, vol. 73, no. 203, pp. 385– 420, 1904.

[23] F. Zhang, et al., "Protein interactions studied by SAXS: Effect of ionic strength and protein concentration for bsa in aqueous solutions". Journal of Physical Chemistry B, 111 (1):251-259, 2007.

[24] J. Rioult et al., "Autonomous electromagnetic mapping system in augmented reality", Int. Symp. on Electromagnetic Compatibility - EMC Europe, 2019.

[25] Wane, S. "ASIC-Correlators with Embedded Cognition for Smart OTA Test", EMC and OTA Tests of Wireless Devices in Reverberation Chambers, EMC-Europe 2021, online workshop: https://www.emc2021.emcss.org/assets/images.

[26] V. Fernandez-Hurtado, et a., "Exploring the limits of super-planckian far-field radiative heat transfer using 2D materials". ACS Photonics, 5(8):3082–3088, 2018.

[27] M. Planck, "The Theory of Heat Radiation" (P. Blakiston's Son & Co., Philadelphia, 1914).

[28] Denis Tihon, et al., "Modal characterization of thermal emitters using the Method of Moments", EuCAP, 2020, Page(s)1-5.